Performance of normal-incidence molybdenum–yttrium multilayer-coated diffraction grating at a wavelength of 9 nm

Benjawan Sae-Lao, Saša Bajt, Claude Montcalm, and John F. Seely

The first experimental investigation of a normal-incidence Mo–Y multilayer-coated diffraction grating operating at a 9-nm wavelength is reported. The substrate is a replica of a concave holographic ion-etched blazed grating with 2400 grooves/mm and a 2-m radius of curvature. The measured peak efficiency in the −3 order is 2.7% at a wavelength of 8.79 nm. To our knowledge, this is the highest normal-incidence grating efficiency ever obtained in this wavelength region.

OCIS codes: 050.0050, 050.1950, 230.4170, 310.6860, 340.7470, 350.1260.

1. Introduction

There has been a continuing effort in the development of normal-incidence multilayer coatings for extreme-ultraviolet (EUV) solar and astrophysical instruments such as telescopes and spectrographs. The high reflectance and wavelength-selective properties of multilayer-coated optics allow imaging and recording of distinct emission lines from solar regions. The solar coronal image dominated by the Si XII at 4.4 nm, recorded during a rocket flight on October 1985 by a W–C multilayer-coated telescope, represents the first successful use of multilayer technology for astrophysical observation.[1] Recent images of the Sun obtained from the Solar and Heliospheric Observatory (SOHO)[2] and Transition Region and Coronal Explorer (TRACE)[3] missions have been made possible with the application of Mo–Si and Mo_2C–Si multilayer coatings, respectively. The operational wavelength of these multilayers was optimized to 17.1 nm, 19.5 nm, 28.4 nm, and 30.4 nm for the selected emission lines of Fe IX/X, Fe XII, Fe XV, and He II, respectively. Such observations provide sensitive temperature diagnostics in the range from 10^4 to 10^6 K and also the detailed information about conditions on the Sun, including plasma confinement, plasma heating, and solar flares. Multilayers were also applied on various types of grating to enhance the grating efficiency, especially for high-resolution spectroscopy of weak EUV sources. Gratings with Mo–Si multilayer coatings operating in a region above the Si L edge at 12.4 nm have substantially higher efficiency than typical gold-coated gratings.[4–7] Recently, MoRu–Be multilayers enabled grating operation at normal incidence with efficiencies of up to 10.4% in the 11.1–12.0-nm wavelength region.[8,9] However, there are still interesting portions of the EUV spectrum that have not yet been explored[10] and that cannot be accessed by the above-mentioned multilayers.

According to the all-sky survey conducted in the 7–80-nm wavelength region by the Extreme Ultraviolet Explorer mission,[11] there are over 700 bright objects in space, including hot white dwarfs, active and nearby late-type stars, cataclysmic variables, and various types of active galactic nuclei, that radiate EUV energy. In the 8–12-nm spectral range, the most intense emission line is Fe XVIII at 9.392 nm. This line was observed in rotating cool stars and white dwarf systems and can be used, for example, to study magnetic fields. It is therefore of interest to develop high-resolution spectroscopic instruments based on high-efficiency diffraction gratings that operate in this wavelength region. Experimental data on multilayers that can reflect at 9.4 nm at normal incidence include the Mo–Sr, Mo–Y, Ru–C, Pd–B_4C, Cr–C, and W–B_4C material pairs.[12]

When this research was performed, B. Sae-Lao (saelao@llnl.gov), S. Bajt, and C. Montcalm were with Physics and Advanced Technologies, Lawrence Livermore National Laboratory, P.O. Box 808, L-395, Livermore, California 94551. C. Montcalm is now with Veeco-Ion Tech, 2330 East Prospect, Fort Collins, Colorado 80525. B. Sae-Lao is also with the Department of Applied Science, University of California, Davis, California 95616. J. F. Seely is with the Space Science Division, U.S. Naval Research Laboratory, Code 7674, Washington, D.C. 20375.

Received 5 November 2001; revised manuscript received 5 February 2002.

However, to our knowledge, none of these multilayers was ever applied to a grating. Theoretical calculations predict much higher reflectance for Mo–Sr and Mo–Y multilayers than for the other multilayer pairs mentioned above. Even though Mo–Sr theoretical reflectance is the highest in this group, the experimental data revealed that this multilayer, if exposed to air, would completely loose its reflective properties within one day because of oxidation.[13] Therefore we limited our study on Mo–Y multilayers, which provide substantially high reflectance and long lifetime.[14]

In this paper we investigate the performance of a Mo–Y multilayer-coated diffraction grating operating at 9 nm. The grating principle and fabrication procedure are explained in Section 2. The multilayer deposition techniques and the characterization techniques used in this study are described in Sections 3 and 4, respectively. The experimental results and discussions are presented in Section 5, followed by a comparison between the measured and the calculated grating efficiencies in Section 6. The conclusions are discussed in Section 7.

2. Grating Operation and Fabrication

Diffraction gratings are commonly used in spectroscopic instruments to disperse polychromatic light. The grating diffracts light into several orders given by the grating equation:

$$m\lambda = d(\sin\alpha - \sin\beta), \tag{1}$$

where m is the grating order; d is the groove spacing; α and β are the incidence angle and the diffraction angle measured from the grating normal, respectively; and λ is the wavelength of light. The efficiency at each order depends strongly on the grating profile. The efficiency of one particular order can be maximized with use of a blazed (sawtooth) line profile. The blaze angle ϕ_b is chosen so that the facets reflect light of a particular wavelength into the chosen diffracted order, which means that blazed gratings have a high peak efficiency at only specific wavelengths. The grating efficiency also depends on the quality of the line profile and the smoothness of the grating surface. For an on-blaze operation, the wavelength in the m grating order can be expressed as

$$\pm m\lambda = 2d \sin\phi_b \sin\theta, \tag{2}$$

where $\theta = \pi/2 - \alpha \pm \phi_b = \pi/2 - \beta \pm \phi_b$ is the grazing-incidence angle that corresponds to the facet normal (Fig. 1).

Let us now consider multilayer-coated gratings. Typical multilayers consist of a periodic stack of two alternating materials having high and low indices of refraction. When we use the well-known quarter-wave stack idea[15] and ignore the absorption, the maximum reflectance occurs when the optical thickness of each layer is equal to a quarter of the wavelength of interest. In general, the refraction-corrected multi-

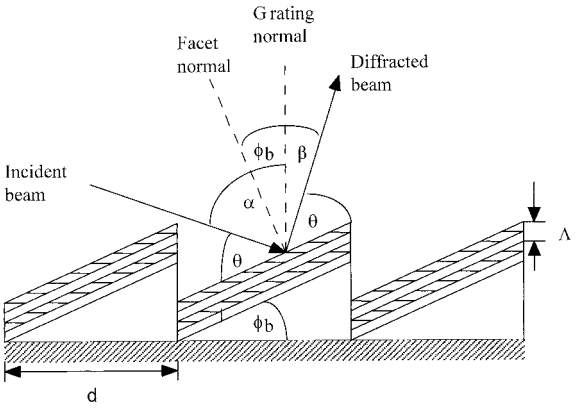

Fig. 1. Schematic drawing of the multilayer blazed grating.

layer period Λ can be determined through the modified Bragg's equation developed by Henke *et al.*[16]:

$$n\lambda = 2d_{\text{Bragg}}(1 - \delta/\sin^2\theta)\sin\theta = 2\Lambda \sin\theta, \tag{3}$$

where $n\lambda = 2d_{\text{Bragg}} \sin\theta$ is the well-known Bragg's law, n is the diffraction order, and δ is the decrement of the average refractive index of the multilayer. For the first-order multilayer interference at normal incidence, the optimum efficiency of an on-blaze operation of a multilayer-coated grating occurs when the blaze wavelength of the grating is equal to the peak wavelength of the multilayer. The following condition must be satisfied to achieve this:

$$\Lambda = d_{\text{Bragg}}(1 - \delta) = \pm d(\sin\phi_b)/m. \tag{4}$$

This condition relates the multilayer period with the diffraction order of the grating. It implies that the maximum efficiency is dependent on λ. Only in the region away from characteristic absorption edges of multilayer materials, where δ is nearly constant, will the grating order remain constant with the change of wavelength.

In this study, a replica of a master holographic blazed grating produced by Spectrogon US Inc. with 2400 groves/mm was coated. The grating was concave with a 2-m radius of curvature. The master grating was produced by a holographic process, in contrast to classical gratings that are mechanically ruled with a diamond tip. A photosensitive layer deposited on top of a glass substrate was exposed with the interference pattern formed by two laser beams, the film was selectively dissolved, and ion-beam etching was used, which made it possible to produce almost sawtooth shaped grooves. The replica gratings, having almost equivalent properties and quality to the master grating, were made by Hyperfine Inc. The aluminum oxide surface resulting from the replication process was coated with a thin SiO_2 layer to reduce the microroughness of the oxidized aluminum surface.

3. Multilayer Deposition

An ultrahigh-vacuum magnetron-sputtering deposition system was used for the fabrication of Mo–Y

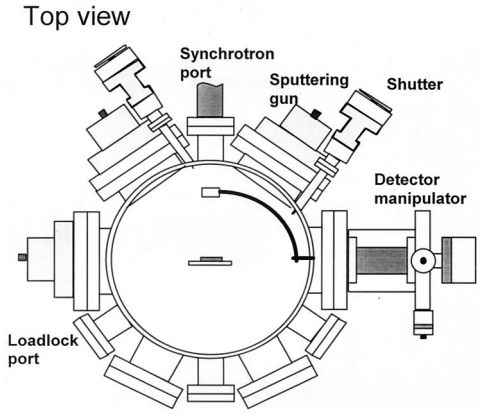

Fig. 2. Schematic drawing of the ultrahigh-vacuum magnetron-sputtering deposition system.

multilayers. A schematic (top view) of the deposition chamber is shown in Fig. 2. Three planar-magnetron-sputtering guns are mounted vertically on the chamber wall. Two are typically used for a multilayer fabrication, and the third one is sometimes used for the deposition of the capping layer of some other material. These sputtering guns were operated at 50 W for both Mo and Y. The shutters in front of each gun were used to regulate the deposition flux. The typical base pressure after a bakeout and prior to deposition was 2×10^{-9} Torr. Ultrahigh purity Ar (99.999%) gas was used at 2.0-m Torr operating pressure and a flow of 40 SCCM (SCCM denotes cubic centimeters per minute at STP). The substrate, placed in the center of the chamber, was mounted on a rotary feedthrough attached to the top chamber lid. The substrate-to-target distance could be varied from 7.5 to 15.5 cm. A substrate of up to 1 cm $\times$ 1 cm in area could be inserted in the chamber through the loadlock system. However, the substrate holder could accommodate a substrate up to 3.5 cm $\times$ 4.5 cm if the chamber was vented.

We deposited a multilayer by facing the substrate alternatively to the Mo and the Y targets and by opening the associated shutter for a predetermined time. Given that the sputtering rates are constant, one can calibrate the deposition rate of each material by making a series of multilayers using different sputtering times. The substrate was spun around its center to achieve good thickness uniformity. Every multilayer in this study started with Y and finished with the Mo layer.

4. Sample Characterization

A. Rutherford Backscattering Spectrometry

Yttrium metal is known to oxidize in air, thus it is crucial to know accurately its composition and density that are the main parameters for the determination of the optical constants used for multilayer design and simulation. Rutherford backscattering spectrometry, a nondestructive depth-profiling technique, was used in this study to determine the oxygen content and any other trace elements in our magnetron-sputtered Y films. A 50-nm-thick Y film was bombarded with 2.3-MeV He^{++} ions, and the energies of the backward-scattered ions were measured at 108° and 170° angles. The energy of the backscattered ions is directly related to the depth and the mass of the target atom, and the number of the backscattered particles is proportional to the atomic concentration. The detection limits range from a few parts per million for heavy elements to a few percent for light elements.

B. X-Ray Diffraction

Small-angle x-ray diffraction (XRD) was applied to determine the period thickness of the multilayers. A collimated beam of Cu K_α x ray with a wavelength of 0.154 nm was incident on a sample, and the diffracted beam was measured specularly. The diffracted beam intensity was measured as a function of the grazing angle 2θ, the angle between the incident and the diffracted beam, over the angular range of $2\theta = 0°$ to 12°. The angular positions of the diffracted peaks are related to the geometric period thickness of the multilayer (d_{Bragg}) to the modified Bragg's formula [Eq. (3)], which was rewritten in the following form:

$$1/d_{\mathrm{Bragg}} = 1/\Lambda(1 - \delta/\sin^2\theta), \tag{5}$$

where Λ can be determined from a linear regression of $1/d_{\mathrm{Bragg}}$ versus $1/\sin^2\theta$. The slope is equal to $-\delta/\Lambda$ with a y-axis interception of $1/\Lambda$.

A series of Mo–Y multilayers of various thickness combinations were fabricated on Si wafer substrates for calibration. With the known deposition times and the calculated period thicknesses obtained from the modified Bragg's equation, we determined the deposition rates of Mo and Y using a two-layer model:

$$\Lambda = r_{\mathrm{Mo}}t_{\mathrm{Mo}} + r_{\mathrm{Y}}t_{\mathrm{Y}} + \Delta\Lambda, \tag{6}$$

where r is the deposition rate, t is the deposition time, and $\Delta\Lambda$ is the change (contraction or expansion) in the period thickness that is due to interface formation. Crystalline structures of Mo and Y in the multilayer were also characterized by large-angle XRD, where the diffracted beam intensity was scanned over the angular range of $2\theta = 30°$ to 50°.

C. Atomic Force Microscopy

We used an atomic force microscope (AFM) (Digital Instruments, dimension 5000) to measure the grating groove profile by scanning a sharp tip mounted on a flexible cantilever over the grating surface. We performed the measurements in a tapping mode by tapping the surface with an oscillating probe tip. The probe tip was etched silicon with a nominal tip radius of 5–10 nm. The AFM measurements were done in air before and after the multilayer coating. A number of scans were performed over the square areas of 1 and 5 μm in the center and near the edge of the grating.

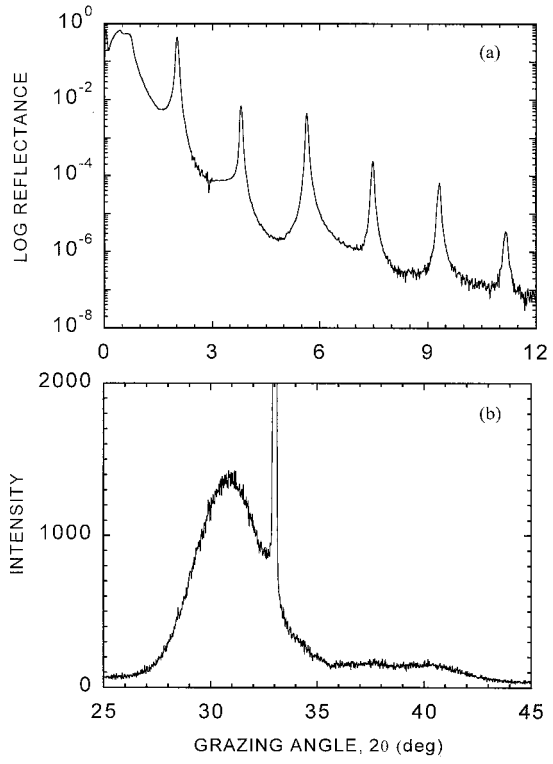

Fig. 3. Typical XRD spectrum of a Mo–Y multilayer measured (a) at small grazing incidence angles from 0° to 12° and (b) at large grazing angles from 25° to 45°. The sharp peak at approximately 33° is the Si peak from the single-crystal ⟨100⟩ substrate.

D. Synchrotron-Based Reflectometry

We measured the multilayer reflectance and the grating efficiency using the reflectometer at beamline 6.3.2 of the Advanced Light Source at Lawrence Berkeley National Laboratory. A detailed description of this beamline can be found elsewhere.[17,18] In this experiment, we used a boron filter and an order suppressor consisting of three grazing-incidence graphite mirrors to improve the spectral purity by suppressing the higher-order light. A GaAsP photodiode with a 5 mm × 5 mm active area served as a detector. The precision of the wavelength and the reflectance measurements were within 0.002 nm and 0.2% (absolute), respectively.

5. Experimental Results and Discussion

Mo–Y coatings exhibit a high-quality multilayer structure. A series of well-defined peaks obtained from small-angle XRD of a typical multilayer [Fig. 3(a)] indicates sharp interfaces between Mo and Y, in good agreement with a small contraction of 0.055 nm obtained from a rate calibration with a two-layer model. The deposition rates of Mo and Y in this study were 0.052 and 0.095 nm/s, respectively. The large-angle XRD spectrum shown in Fig. 3(b) exhibits a peak at $2\theta = 31.19°$, which corresponds to the Y ⟨002⟩ crystalline orientation. However, the peak is rather broad, indicating a polycrystalline structure of Y. In contrast, Mo is predominantly amorphous because no peak is observed.

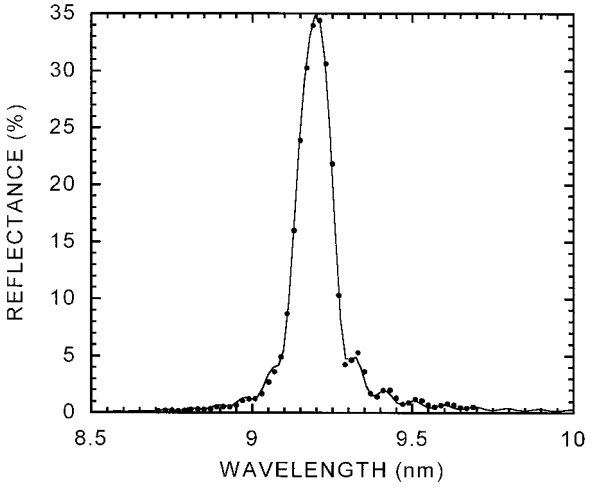

Fig. 4. Normal-incidence (measured 3° from normal) reflectance of a Mo–Y multilayer deposited on a flat Si wafer substrate. Experimental data (dots) and the best fit (solid curve) are shown.

We based the multilayer design on calculations using IMD software[19] assuming an ideal Mo–Y structure. The optimized parameters include the period thickness Λ, the thickness ratio of Mo to the period thickness Γ, and the number of bilayers N. Theoretically, Γ of 0.425 and $N = 120$ bilayers would provide the highest-reflectance Mo–Y multilayer in the 8–12-nm wavelength region. The increase in reflectance with number of bilayers is limited by absorption because light penetrating too deep in the multilayer can no longer reflect to the top surface. This optimum number of N in reality was even lower because of surface–interface roughness of the multilayer that reduces the specular reflectance. The experimental optimum number of bilayers for Mo–Y seemed to be 100, and thus multilayers having only 100 bilayers were made. The reflectance of a Mo–Y multilayer deposited on a flat Si wafer was 34.6% at 9.196 nm when we used the designed parameters $\Lambda = 4.67$ nm, $\Gamma = 0.425$, and $N = 100$ bilayers. Figure 4 shows also the best fit to the measured reflectance of this multilayer. We performed the fit using IMD software, and the optical constants were derived from the Center for X-Ray Optics atomic scattering factors.[20] Instead of bulk Y density (4.457 g/cm^3), we used 4.402 g/cm^3 as measured with Rutherford backscattering spectrometry for our Y films. Lower density can be explained with a high percentage of oxygen (25%) and some other contaminants (1% Ar and 0.3% Ta). The best fit was obtained with $\Lambda = 4.68$ nm, $\Gamma = 0.445$, $N = 100$ bilayers, and the interface roughness of 0.55 nm, in good agreement with our designed parameters. The interface roughness in the fit was assumed to be the same for each interface. Because of the space limitation and the deposition geometry, we could not coat the grating and the flat substrate simultaneously. Thus the reflectance of the coating on the grating was inferred from the above fitting parameters.

AFM images of the grating before and after the

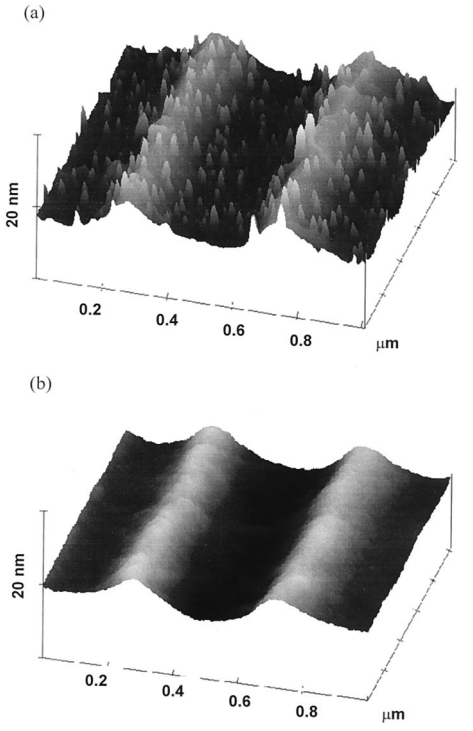

Fig. 5. AFM images (1 μm × 1 μm) of the grating (a) before and (b) after application of the Mo–Y multilayer coating.

application of the Mo–Y coating with optimized deposition parameters are compared in Fig. 5. The vertical scale was adjusted to clearly reveal the texture of the grating image. Numerous spikes present on the substrate grating were smoothed out after the multilayer coating. The microroughness in the $4-40\text{-}\mu\text{m}^{-1}$ spatial frequency, excluding the low-frequency roughness from the groove pattern, was improved from 1.24- to 0.73-nm rms roughness. The smoothing properties of the Mo–Y multilayer enhanced the reflectance and also substantially increased the grating efficiency without degrading the grating performance or affecting the blazed angle.

We measured the grating efficiency using synchrotron radiation in the usual configuration described in Subsection 4.D with an additional 1.49-mm slit added in front of the detector. Grating efficiency is defined as the ratio of the diffracted intensity and the incident intensity, in which the incident radiation is monochromatic. Because this is a reflected-type grating, measuring the diffracted intensity is the same as measuring the reflected intensity. At fixed incident angles, the wavelength was scanned after the zero grating order was established. Approximately 0.89% grating efficiency at an 8.85-nm wavelength was measured at 8° from normal. This result implies that a higher grating efficiency could be obtained at 9.4 nm because of the increase of multilayer reflectance with wavelength in this spectral range. In Fig. 6 the measured zero-order efficiency at a normal-incidence angle of 8° is shown together with the predicted reflectance curve. This Mo–Y multilayer-coated grating had approximately 2.8%

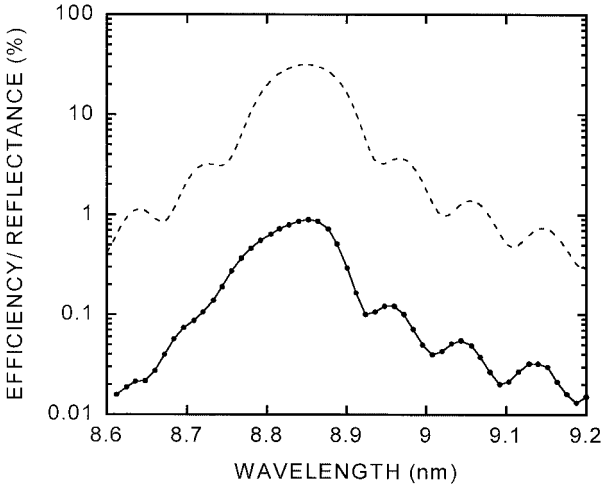

Fig. 6. Zero-order grating efficiency measured at 8° from normal incidence (dotted curve) and the predicted reflectance (dashed curve) of the witness Mo–Y multilayer coating obtained from the fit.

groove efficiency in the zero order at an 8.85-nm wavelength where the grating's groove efficiency is defined as the ratio of the grating efficiency and the coating reflectance. For a fixed wavelength, by scanning the detector around the specular angle where zero-order diffraction is located, we measured the efficiencies in various diffraction orders as displayed in Fig. 7. The positive-order numbers indicate the inside order, with the diffraction angle lying between the incident beam and the zero order, as opposed to the outside order. To optimize for peak efficiency of each order, the wavelength was scanned after the detector was aligned at peak angle. As shown in Fig. 8, the peak efficiencies as a function of wavelength were measured at 8° from normal incidence. The highest efficiency was 2.7% in the outside third order ($m = -3$) at a wavelength of 8.79 nm. To our knowledge, this is the highest efficiency ever obtained at normal incidence in this wavelength region. Without the Mo–Y multilayer, the grating efficiency would have been zero (below the detection limit). The Mo–Y multilayer dramatically increased the grating efficiencies and enabled the grating to operate in this wavelength region.

6. Calculated Grating Efficiency

The multilayer grating efficiency was calculated with the computational model PCGrate developed by Goray and colleagues.[21,22] The computational model implements the modified integral method to solve the boundary-value problem of electromagnetic radiation incident on a multilayer grating. The calculation accounts for the groove profile of the grating substrate as determined by an AFM, the optical properties of the layers of the multilayer coating,[20] and the two polarization components of the incident radiation. The computational model was previously used to analyze the efficiency of MoRu–Be multilayer gratings of the same type as used in this study.[9]

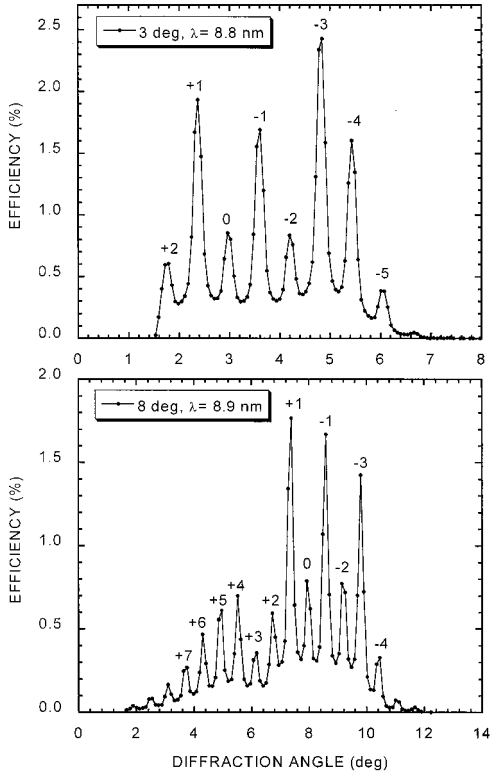

Fig. 7. Efficiencies of the grating measured in various diffraction orders at 3° and 8° normal-incidence angles.

The calculated efficiencies are shown in Fig. 9. The calculated peak efficiency in the −3 order is in good agreement with the measured peak efficiency. The calculated efficiencies of the weaker orders in some cases differ from the measured efficiencies in the same manner as found previously in Ref. 9. As discussed in Ref. 23, these differences indicate that the treatment of the microroughness in the computational model needs improvement, and this research is in progress.

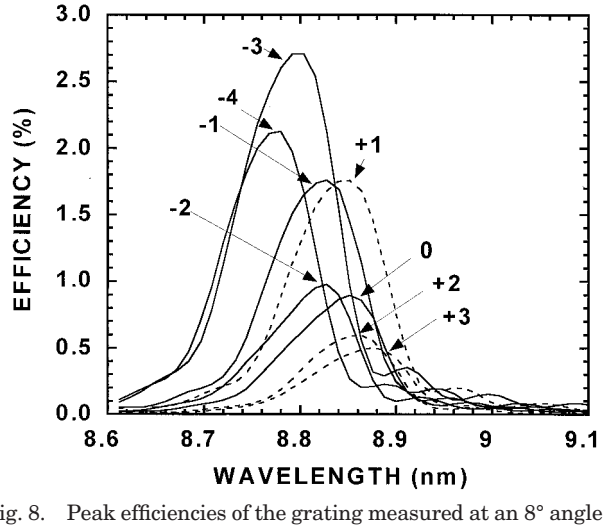

Fig. 8. Peak efficiencies of the grating measured at an 8° angle of incidence as a function of wavelength. The highest measured efficiency was 2.7% in the −3 order at a wavelength of 8.79 nm.

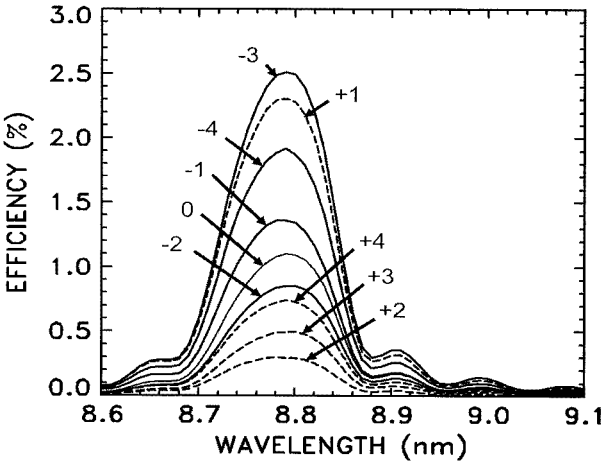

Fig. 9. Grating efficiencies calculated for an 8° angle of incidence as a function of wavelength.

7. Conclusion

We have reported on the enhancement of the normal-incidence efficiency of a blazed holographic grating by the application of a Mo–Y multilayer coating. The measured peak efficiency in the −3 order was 2.7% at a wavelength of 8.79 nm and is the highest normal-incidence efficiency measured in this wavelength region to our knowledge. The measured efficiency is high enough to make possible the utilization of multilayer gratings for high-resolution spectroscopic studies of solar and astrophysical objects in the 9-nm wavelength region. A flight instrument using such a grating could perform Doppler imaging that would reveal the magnetic fields and the structure of active regions. In addition, the spectra dispersed by the grating could be used to perform other studies such as solar abundances.

The authors thank Jay Ayers and Rick Levesque, Lawrence Livermore National Laboratory (LLNL), for their help in the design and fabrication of the sample holder. Special thanks go to Eric Gullikson, Lawrence Berkeley National Laboratory (LBNL), for helpful guidance in grating characterization and to Sherry Baker (LLNL) for the AFM measurements. This research was performed under the auspices of the U.S. Department of Energy by the University of California Lawrence Livermore National Laboratory under contract W-7405-ENG-48. Funding was partially provided by NASA project W-19513.

References and Notes

1. M. E. Bruner, B. M. Haisch, W. A. Brown, L. W. Acton, and J. H. Underwood, "Soft x-ray images of the solar corona using normal incidence optics," J. Phys. (Paris) Suppl. **49,** 115–118 (1988).
2. Information on the SOHO mission is available at http://sohowww.nascom.nasa.gov.
3. Information on the TRACE mission is available at http://vestige.lmsal.com/TRACE/.

4. J. F. Seely, R. G. Cruddace, M. P. Kowalski, W. R. Hunter, T. W. Barbee, J. C. Rife, R. Ely, and K. G. Stilt, "Polarization and efficiency of a concave multilayer grating in the 135–250-Å region and in normal-incidence and Seya–Manioc mounts," Appl. Opt. **34,** 7347–7354 (1995).
5. J. F. Seely, M. P. Kowalski, R. G. Cruddace, K. F. Heidemann, U. Heizmann, U. Kleineberg, K. Osterried, D. Menke, J. C. Rife, and W. R. Hunter, "Multilayer-coated laminar grating with 16% normal-incidence efficiency in the 150-Å wavelength region," Appl. Opt. **36,** 8206–8213 (1997).
6. J. F. Seely, M. P. Kowalski, W. R. Hunter, J. C. Rife, T. W. Barbee, G. E. Holland, C. N. Boyer, and C. M. Brown, "On-blaze operation of a Mo/Si multilayer-coated concave diffraction grating in the 136–142-Å wavelength and near normal incidence," Appl. Opt. **32,** 4890–4897 (1993).
7. J. F. Seely, M. P. Kowalski, W. R. Hunter, T. W. Barbee, R. G. Cruddace, and J. C. Rife, "Normal-incidence efficiencies in the 115–340-Å wavelength region of replicas of the Skylab 3600 line/mm grating with multilayer and gold coatings," Appl. Opt. **34,** 6453–6458 (1995).
8. C. Montcalm, S. Bajt, and J. F. Seely, "MoRu–Be multilayer-coated grating with 10.4% normal-incidence efficiency in the 11.4-nm wavelength region," Opt. Lett. **26,** 125–127 (2001).
9. J. F. Seely, C. Montcalm, S. Baker, and S. Bajt, "High-efficiency MoRu–Be multilayer-coated gratings operating near normal incidence in the 11.1–12.0-nm wavelength range," Appl. Opt. **40,** 5565–5574 (2001).
10. U. Feldman, P. Mandelbaum, J. F. Seely, G. A. Doschek, and H. Gursky, "The potential for plasma diagnostics from stellar extreme ultraviolet observation," Astrophys. J. Suppl. **81,** 387–408 (1992).
11. Information on the EUVE mission and the observed spectral lines can be obtained at http://ssl.berkeley.edu/euve.
12. Reports of measured multilayer reflectances are available at http://www-cxro.lbl.gov/multilayer/survey.html.
13. B. Sae-Lao and C. Montcalm, "Molybdenum-strontium multilayer mirrors for the 8–12-nm extreme-ultraviolet wavelength region," Opt. Lett. **26,** 468–470 (2001).
14. C. Montcalm, B. T. Sullivan, M. Ranger, and H. Pépin, "Ultra-high vacuum deposition-reflectometer system for the in situ investigation of Y/Mo extreme ultraviolet multilayer mirrors," J. Vac. Sci. Technol. A **15,** 3069–3081 (1997).
15. E. Spiller, *Soft X-Ray Optics*, Vol. PM15 of the SPIE Press Monographs (SPIE, Bellingham, Wash., 1994).
16. B. L. Henke, J. Y. Uejid, H. T. Yamada, and R. T. Tackaberry, "Characterization of multilayer x-ray analysers: model and measurements," Opt. Eng. **25,** 937–947 (1986).
17. J. H. Underwood and E. M. Gullikson, "High-resolution, high-flux, user friendly VLS beamline at the ALS for the 50–1300 eV energy region," J. Electron Spectrosc. Relat. Phenom. **92,** 265–272 (1998).
18. E. M. Gullikson, S. Mrowka, and B. B. Kaufmann, "Recent developments in the EUV reflectometry at the Advanced Light Source," in *Emerging Lithographic Technologies V*, E. A. Dobisz, ed., Proc. SPIE **4343,** 363–373 (2001).
19. D. L. Windt, "IMD: software for modeling the optical properties of multilayer films," Comput. Phys. **12,** 360–370 (1998); a copy of the software can be downloaded at http://cletus.phys.columbia.edu/~windt/imd/.
20. B. L. Henke, E. M. Gullikson, and J. C. Davis, "X-ray interactions: photoabsorption, scattering, transmission, and reflection at E = 50–30,000 eV, Z = 1–92," At. Data Nucl. Data Tables **54,** 181–342 (1993); these data are also available in electronic form at http://www-cxro.lbl.gov.
21. L. I. Goray, "Numerical analysis for relief gratings working in the soft x-ray and XUV region by the integral equation method," in *X-Ray and UV Detectors*, R. B. Hoover and M. W. Tate, eds., Proc. SPIE **2278,** 168–172 (1994).
22. L. I. Goray and B. C. Chernov, "Comparison of rigorous methods for x-ray and XUV grating diffraction analysis," in *X-Ray and Extreme Ultraviolet Optics*, R. B. Hoover, and A. B. C. Walker, eds., Proc. SPIE **2515,** 240–245 (1995).
23. L. I. Goray and J. F. Seely, "Efficiencies of master, replica, and multilayer gratings for the soft x-ray–EUV range: modeling based on the modified integral method and comparisons to measurements," Appl. Opt. **41,** 1434–1445 (2002).